Am J Cancer Res 2024;14(7):3433-3450
www.ajcr.us /ISSN:2156-6976/ajcr0155917

Original Article

THBS2 promotes gastric cancer progression and stemness via the Notch signaling pathway

Zhengyao Chang[1,2*], Yunhe Gao[2*], Peng Chen[2*], Wenxing Gao[1,2], Wen Zhao[2,3], Di Wu[1,2], Wenquan Liang[2], Zhida Chen[2], Lin Chen[2], Hongqing Xi[2]

[1]Medical School of Chinese PLA, Beijing 100853, China; [2]Department of General Surgery, The First Medical Center of Chinese PLA General Hospital, Beijing 100853, China; [3]School of Medicine, Nankai University, Tianjin 300071, China. [*]Equal contributors.

Received February 15, 2024; Accepted June 20, 2024; Epub July 15, 2024; Published July 30, 2024

Abstract: Thrombospondin-2 (THBS2), a secreted extracellular matrix protein, plays a crucial role in various biological processes including angiogenesis, tissue remodeling, and inflammation. Our study focuses on its function in human gastric cancer (GC). Through bioinformatics and tumor tissue analysis, we compared THBS2 expression in GC tissues and adjacent tissues, and predicted regulatory upstream and downstream molecules. The direct regulatory effect of miR-29b-3p on THBS2 was evaluated through dual-luciferase reporter assays, showing that miR-29b-3p targets the 3'-UTR of THBS2 mRNA, reducing its expression in GC cells. The influence of THBS2 on tumorigenesis and stemness was examined on protein expression levels via Western blot. In vivo, THBS2's role was investigated through xenograft and metastasis assays in nude mice, demonstrating that downregulation of THBS2 impairs GC tumorigenesis and liver metastasis. Our study identified THBS2 as a highly expressed prognostic factor in GC patients. Functionally, THBS2 promotes GC progression through the Notch signaling pathway by regulating Notch3, NEY1, and HES1 proteins, and sustains cancer stem cell-like characteristics by Notch3, including the expression of CD44, Nanog, OCT4, and SOX2. In sum, our study reveals that THBS2 promotes GC progression and stemness, modulated negatively by miR-29b-3p. This suggests potential therapeutic targets within the THBS2/Notch signaling axis for combating gastric cancer.

Keywords: Gastric cancer, THBS2, miR-29b-3p, Notch signaling pathway, cancer stem cells

Introduction

Gastric cancer (GC) is a significant malignancy and a leading cause of cancer-related mortality worldwide, with more than one million new cases each year, accounting for 5.7% of all cancers [1-3]. Despite various treatment options for GC including surgical intervention, radiation therapy, neoadjuvant chemotherapy, targeted therapy, and immunotherapy, the prognosis remains unsatisfactory. The complex nature of oncogenes and the inherent heterogeneity of GC necessitate targeted research efforts. Effectively identifying therapeutic targets and in-conducting detailed mechanistic studies are crucial for improving management strategies and patient outcomes in GC.

Thrombospondins (THBSs) are a conserved family of extracellular, oligomeric, multidomain, calcium-binding glycoproteins Multidomain, calcium-binding glycoproteins, initially discovered in 1971 by Baenziger et al. [4]. This family members include THBS1 to THBS5, which play critical roles in structural support, cell adhesion, and signaling in the extracellular matrix. They facilitate intercellular and matrix interactions by binding to cell surface receptors, thus regulating fundamental biological processes such as cellular proliferation, migration, and apoptosis [5]. The role of THBS in transitioning from pro-tumorigenic to anti-tumorigenic functions remain controversial. For instance, THBS1 is known to inhibit angiogenesis in the early stage and promotes tumor cell adhesion in the later stage. THBS2 showed high expression during epithelial-mesenchymal transition (EMT), extracellular matrix (ECM) formation, and in invasion and metastasis stages of cancer [6], marking it as a critical regulator of tumorigenesis. The

https://doi.org/10.62347/UXWK4038

overexpression of in cancer tissues is often associated with tumor progression [7-10], and serum levels of THBS2 are considered a valuable clinical marker for various cancers. Consequently, the involvement of THBS2 in multiple types of human cancers highlights its potential as a therapeutic target for suppressing the advancement of GC. Revealing the precise mechanisms underlying its contribution to GC progression and developing appropriate therapeutic strategies remain critically important.

In this study, we validate a strong correlation between elevated THBS2 expression and poor prognosis in GC. We demonstrated that reducing THBS2 expression effectively hinders the proliferation, metastasis, and stem cell characteristics of GC cells, as evidenced by in vitro and in vivo assays. Additionally, we identify the upstream regulator miR-29b-3p and its role in Notch pathway activation, promoting EMT, and enhancing cancer stem cell properties. Taken together, the miR-29b-3p/THBS2/Notch signaling axis may be a promising target for developing novel therapeutic strategies for GC.

Methods

Patients and specimens

Between January 2022 and January 2023, we collected 30 paired specimens of human GC and adjacent non-malignant tissues from the Chinese PLA General Hospital in Beijing, China. None of the patients had undergone adjuvant therapies prior to surgical resection. Postoperative pathological examination confirmed the diagnosis of GC and the normality of adjacent tissues. This study was approved by the Ethics Committee of PLA General Hospital (S2021-022-01) and conducted in accordance with the Declaration of Helsinki.

Cell culture

The GES-1 normal stomach epithelial cell line and seven human GC cell lines were obtained from the Chinese Academy of Sciences Cell Bank (Shanghai, China). These cell lines were cultured in DMEM (GIBCO, NY, USA) supplemented with 10% fetal bovine serum (FBS; PAN-Seratech) and 1% penicillin-streptomycin solution (PS; Sea clone), maintained at 37°C and 5% CO_2.

Spheroid-formation assay

HGC-27 and AGS cell lines were cultured in ultra-low attachment 6-well plates (Corning, NY, USA) using modified DMEM/F12 medium supplemented with 20 ng/mL epidermal growth factor (Peprotech, NJ, USA), 2% B27 supplements (Invitrogen, CA, USA), 1% insulin-transferrin-selenic acid (Corning), 10 ng/mL LIF (Peprotech), 10 ng/mL gastrin I (Peprotech), and 10 ng/mL basic fibroblast growth factor (Peprotech).

RNA extraction, cDNA synthesis, and qRT-PCR

Total RNA was extracted from cell lines or tissues samples using the TRIzol reagent (Invitrogen). For mRNA, cDNA synthesis was performed using SuperScript IV Reverse Transcriptase Kit (Thermo Fisher Scientific, MA, USA), followed by qRT-PCR with PowerUp SYBR Green Master Mix (Thermo Fisher Scientific). For miRNA analysis, cDNA was synthesized using the miRNA 1st Strand cDNA Synthesis Kit, and quantified using miRNA Universal SYBR qPCR Master Mix (Vazyme, Nanjing, China). A CFX96 real-time PCR detection system (Bio-Rad, CA, USA) was employed, with normalized to GAPDH for mRNA and U6 for miRNA. Expression levels were calculated utilizing the 2-ΔΔCT method with triplicates for each sample. All primers used are listed in Supplementary Table 1.

Protein extraction and western blot

Cells were lysed, and protein extracted and quantified using the BCA method protein sepsis assay kit (Solarbio, Beijing, China). Proteins were separated by SDS-PAGE Gel and transferred to polyvinylidene fluoride (PVDF) membranes (Millipore, Darmstadt, Germany), which were blocked with 5% defatted milk for 2 hours at room temperature. Membranes were then incubated overnight with primary antibodies (1:1,000) at 4°C, followed by secondary antibodies (1:4,000) for 2 hours at room temperature. Protein bands were visualized using an ECL chemical fluorescent agent (Beyotime). Details of the antibodies used are provided in Supplementary Table 2.

Cell transfection

HEK293T cells were transfected with packaging plasmids (VSVG and ΔR) and the expres-

sion plasmids (sh-Ctrl/Vector and sh-THBS2/THBS2, Notch3) obtained from GeneChem (Shanghai, China), using Lipofectamine™ 2000 from Invitrogen. Lentiviral particles were produced to infect HGC-27 and AGS cells, employing Polybrene (Solarbio) as the transfection reagent. Stable cell lines with successful infections were selected through screening with Gibco products. Additionally, MiR-29b-3p mimics, inhibitors, and corresponding negative controls (NC) were purchased from GenePharma (Shanghai, China). Cells in 6-well plates were transfected at 30%-50% confluency using Lipofectamine™ 2000. The cells were washed with 1× PBS before being transfected with miR-29b-3p mimic or mimic NC at a concentration of 50 nM for GC cells (HGC-27 and AGS cells), along with inhibitors or inhibitor controls at a concentration of 100 nM using Lipofectamine™ 2000 from Invitrogen.

Immunohistochemistry (IHC)

Deparaffinized and rehydrated tissue sections of 5 μm thickness underwent antigen retrieval in EDTA buffer (pH=8.0), microwaved for 15 minutes. After PBS washes, sections were blocked with 3% BSA and incubated overnight at 4°C with primary antibody THBS2 (#BA3616-2, BOSTER, Wuhan, China). The secondary antibody conjugated with HRP was then incubated for 1 hour at room temperature. The peroxidase reaction was developed using 3,3-diaminobenzidine (DAB) and the slides were counterstained with hematoxylin. Images were captured and analyzed using a microscope.

Cell proliferation (CCK-8 assay)

The GC cells were seeded at 2,000 cells per well in 100 μL in 96-well plates. Each experimental group and blank control group comprised of three replicate wells. After adding 10 μL of CCK-8 reagent (Solarbio) to each well, the plates were incubated for an hour at 37°C under a 5% CO_2 atmosphere. Cell viability was assessed at 0, 24, 48, and 72 hours by reading the optical density at 450 nm using a microplate reader.

Colony formation assay

To assess the viability of GC cells, both experimental and control group cells were seeded in 6-well plates (1×10^3 cells/well) and incubated at 37°C with 5% CO_2 for two weeks. Once colonies were visible formed, they were fixed with 4% paraformaldehyde for 30 minutes and stained with crystal violet for 15 minutes. The colonies were quantified and documented using a digital camera.

Flow cytometry analysis

Apoptosis Detection: Cells were trypsinized without EDTA, rinsed with chilled PBS, and resuspended in 500 μL of Binding Buffer at approximately 5×10^5 cells per sample. Annexin V-FITC (5 μL) and PI (10 μL) were added, and the cells were incubated at room temperature in the dark for 5 minutes before apoptosis analysis using a BD flow cytometer (BD LSRII).

Cell Cycle Analysis: Cells ranging from 2×10^5 to 1×10^6 were collected, washed with PBS, and the supernatant was discarded after centrifugation. DNA Staining solution (1 ml) and Permeabilization solution (10 μL) were then added to cell suspension for incubation at room temperature in the dark for 30 minutes. Cell cycle analysis was performed using a BD flow cytometer.

CD44 Expression Levels: 1×10^6 cells were washed with PBS, and resuspended in 100 μL PBS and incubated with PE-Cy7 Mouse Anti-Human CD44 (#560533, BD Biosciences, CA, USA) on ice in the dark for 30 minutes. After further PBS washes, CD44 expression levels were determined using a BD flow cytometer. Data analysis was performed using FlowJo software (version 10; Tree Star Inc., USA).

Wound healing assay

GC cells were cultured in six-well plates until reaching 90% confluency. A wound was created with a 200 μL pipette tip in the culture dish. The wells were gently washed with PBS to remove detached cells and debris. The medium was replaced with a serum-free variant to inhibit proliferation. The wound closure was recorded and evaluated at intervals of 6, 12, 18, 24, and 48 hours by calculating the reduction in distance from the original wound edge. Images were captured at 0 and 48 hours using a 10× microscope. Data are presented as mean ± SD.

Transwell migration and invasion assays

For migration assays, $4\text{-}5\times10^4$ cells were suspended in 200 μL serum-free medium and

placed into an 8 μm pore size transwell chamber (Corning, USA). The lower chamber was filled with 800 μL medium containing 20% FBS. In invasion assays, each chamber was precoated with a 1:9 diluted mixture of Matrigel (Corning) and medium using 50 μL. A cell suspension of 1-2×10^5 cells in 200 μL serum-free medium was added to the coated chambers, and 800 μL of medium containing 20% FBS was added to the lower chamber. After 24 hours of incubation at 37°C with 5% CO_2, non-migrated or non-invaded cells in the upper chambers were removed with cotton swabs. Cells that adhered to the bottom surface of the chambers were fixed with 4% paraformaldehyde (PFA) for 15 minutes and stained with crystal violet for 30 minutes. Cells were then visualized and counted under a microscope.

Luciferase reporter gene assay

The interaction between miR-29b-3p and THBS2 was explored using a luciferase reporter gene assay. HEK293T cells were co-transfected with THBS2 wild type/mutant plasmids bearing a renaline luciferase reporter gene and miR-29b-3p mimics or controls in 24-well plates using Lipo6000TM transfection reagent. Luciferase activity was measured 48 hours post-transfection using the Dual-Glo® Luciferase Assay System (Promega, WI, USA) according to the manufacturer's instructions.

Bioinformatics analysis

The gene expression dataset of GC was retrieved from GEO database (http://www.ncbi.nlm.nih.gov/geo/). Differential expressed genes (DEGs) were analyzed by GEO2R (http://www.ncbi.nlm.nih.gov/geo/geo2r/). Protein-protein interaction (PPI) networks were constructed using the STRING database (http://string.embl.de/) and visualized with Cytoscape software. OncoPrints were generated from c-BioPortal database (http://cbioportal.org). Predictions of miRNAs targeting THBS2 were made using TargetScan (http://www.targetscan.org/vert_2/), Starbase (http://starbase.sysu.edu.cn/-index.php), miRDB (http://mirdb.org/), and miRWALK (http://mirwalk.umm.uni-heidelberg.de/) databases, with overlapping results visualized using Venn diagrams (https://jvenn.toulouse.inrae.fr/app/example.html) from Jvenn. The Cancer Genome Atlas (TCGA) and GEO (NCBI) databases were employed to analyze THBS2 and miR-29b-3p expression levels in both GC and adjacent normal tissues. Survival outcomes were assessed using Kaplan Meier plotter analysis (http://kmplot.com/analysis/index.php). Correlations between miRNAs expression and target gene levels were analyzed based on TCGA database.

Chemical substances

The γ-secretase inhibitor DAPT (#S2215, Selleck, TX, USA) was prepared as a 10 mM stock solution. For in vitro experiments, an effective working concentration of 75 μM was determined.

In vivo experiments

5-week-old nude mice (n=5/group) used for animal experiments were procured from the Shanghai Model Organisms Center (Shanghai, China). For tumor growth studies, sh-Ctrl/HGC-27 and sh-THBS2/HGC-27 cells were subcutaneously injected into mice at a density og 5×10^6 cells per 100 μL of saline. Tumor volume was monitored bi-daily using a vernier caliper. For the liver metastasis model, sh-Ctrl/HGC-27 and sh-THBS2/HGC-27 cells (3 mice/group, 2×10^6 cells/mL; 100 μL per mouse) were injected into spleen. Liver tissues were harvested after 6 weeks for HE staining and IHC. Randomization was employed for animal assignment, and investigators were blinded to group assignments. All procedures adhered to ethical standards for animal care.

Statistical analysis

Statistical analysis was performed using SPSS 25.0 (IBM Corp, Armonk, NY, USA). Survival curves of GC patients were generated using Kaplan-Meier and independent risk factors were analyzed with multivariate Cox regression methods. The quartile method was employed to determine the cutoff value of THBS2 expression for survival analysis, based on TCGA database. Spearman correlation analysis was used to examine the association between THBS2 and miR-29b-3p. Expression comparisons between tumor and non-tumor tissue in GC patients were performed using t-tests. GraphPad Prism 8 software was used for data visualization. Significance thresholds were set at *P < 0.05, **P < 0.01, ***P < 0.001, with "ns" indicating no statistical significance (P < 0.05).

Results

THBS2 expression is upregulated in GC and predicts poor survival

To identify key molecules promoting gastric cancer, we conducted an unbiased screening using bioinformatics methods. Firstly, we downloaded three gene expression microarray datasets (GSE103236, GSE54129 and GSE19826) consist of 1213, 1738, and 1305 differential expressed genes (DEGs), respectively, from GEO database and extracted lists of DEGs between tumor and normal samples for each dataset. To increase the reliability of potential molecules, we intersected these three differentially expressed gene lists, yielding 137 overlapping DEGs (**Figure 1A**). We then employed the STRING database to visualize the PPI network (Supplementary Figure 1A) and constructed a co-expression network of DEGs using Cytoscape software (Supplementary Figure 1B). The MCODE application identified key modules in the network consisting of 23 nodes and 192 edges (Supplementary Figure 1C), and cytoHubba helped pinpoint the top 10 hub genes, including COL1A1, COL18A1, THBS2, COL3A1, COL11A1, BGN, FN1, COL5A2, COL1A2 and COL10A1 (**Figure 1B**). Further analysis using the online c-BioPortal database (http://cbioportal.org) revealed a high mutation rate in hub genes in gastric cancer patients, notably in COL1A2 (12%), COL11A1 (10%), and THBS2 (7%) (**Figure 1C**), with amplification and missense mutation predominating. Subsequent prognosis analysis revealed a close correlation between THBS2 expression and poor outcomes in gastric cancer, underscoring its potential role in GC progression. However, the regulatory mechanisms and pathways underlying the high expression of THBS2 in gastric cancer patients remain unclear and require further investigation for elucidation.

According to TCGA Pan-Cancer (https://portal.gdc.cancer.gov/), THBS2 was found to increase across various types of cancer, with a notable increase in GC relative to the normal tissue adjacent to carcinoma (**Figure 1D**) and higher stages of tumor progression (**Figure 1E**). Furthermore, THBS2 expression was upregulated in GC samples as verified by multiple microarray analysis (GSE27342, GSE13861, GSE118897, GSE103236, GSE54129, GSE19826, GSE33335, GSE13911, GSE26942 datasets) (**Figure 1F**). To investigate the expression of THBS2 in GC, we initially analyzed the levels of THBS2 mRNA in 7 different GC cell lines versus GES-1 (Human Gastric Epithelial Cells), revealing an upregulation of THBS2 (**Figure 1G**). Protein levels assessed by Western blot (WB) corroborated its high expression in most gastric cancer cell lines (**Figure 1H**). Additionally, our findings indicated a significant overexpression of THBS2 in 27 out of the 30 patients examined (**Figure 1I**), with representative patients further validated using WB and IHC techniques (**Figure 1J**, **1K**). Furthermore, the K-M Plotter database was utilized to determine the cutoff value for THBS2 in survival analysis including Overall Survival (OS), First Progression Survival (FPS), and Post Progression Survival (PPS) data. According to the median expression value of THBS2, it was divided into high and low expression, so as to conduct survival analysis. The findings revealing that high THBS2 expression correlates with unfavorable prognosis among GC patients (**Figure 1L**). Multivariate Cox proportional hazards models demonstrated that elevated levels of THBS2 independently predicted poor survival outcomes (Supplementary Table 3). The receiver operator characteristic (ROC) curve demonstrated an area under the curve (AUC) of 0.844, highlighting THBS2's potential as a diagnostic marker for GC (Supplementary Figure 1D). In summary, our findings underscore a significant upregulation of THBS2 in GC and its association with an adverse prognosis, suggesting its utility as a potential therapeutic target and prognostic indicator in gastric cancer.

THBS2 regulates the progression and stemness of GC cells in vitro

To investigate the role of THBS2 on GC progression, we employed lentiviral plasmids to establish stable cell lines with downregulated (sh-THBS2) and upregulated (OE-THBS2) expression levels of THBS2 in HGC-27 and AGS. An empty vector served as the control (sh-Ctrl or Vector). WB and RT-PCR analyses confirmed the efficiency of THBS2 manipulation (**Figure 2A**, **2B**).

Subsequent analysis was conducted to investigate THBS2's biological function in metastasis of HGC-27 and AGS cells. Migration and invasion assays revealed that reduced THBS2

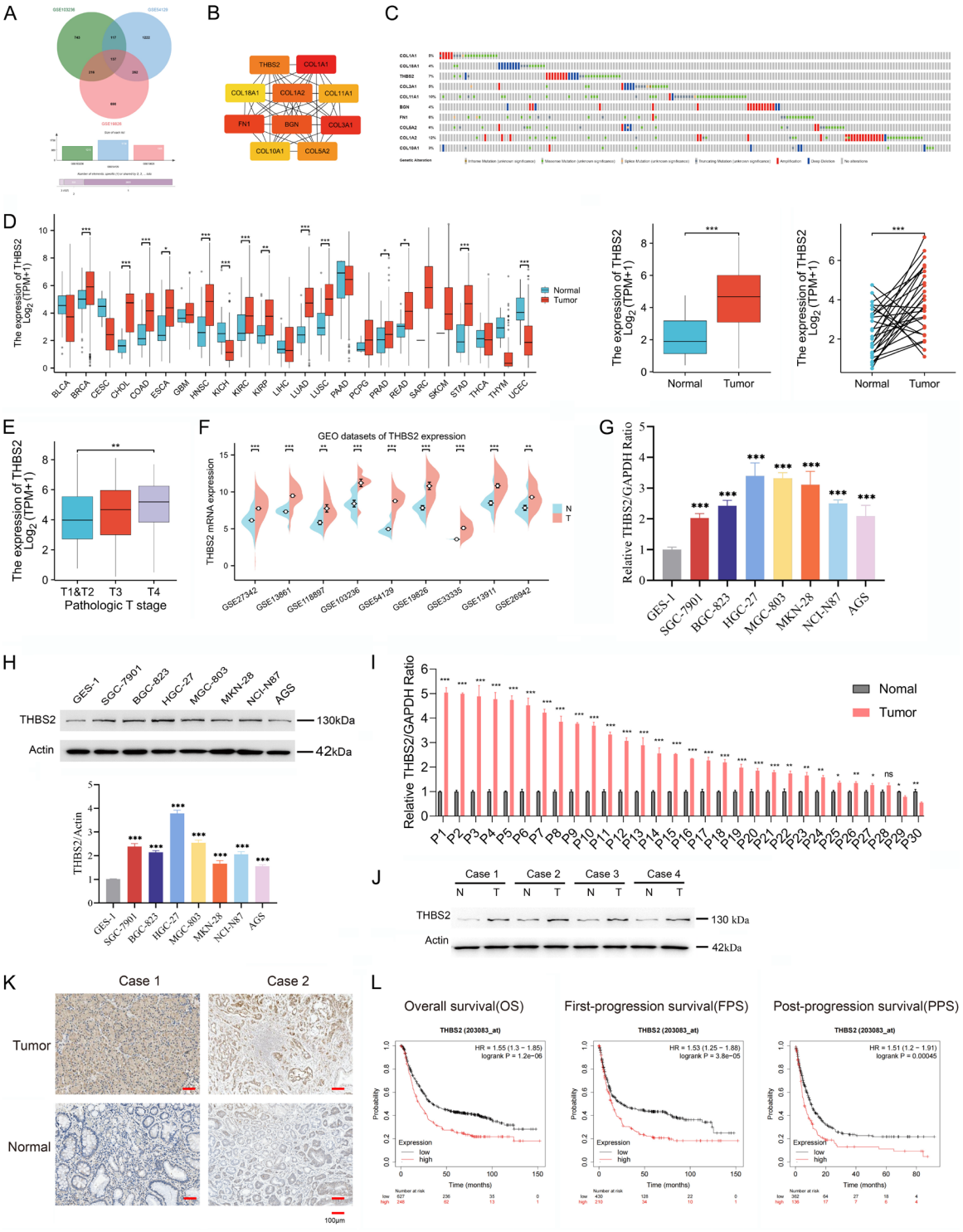

Figure 1. THBS2 expression is upregulated in GC and predicts poor survival in GC patients. A. A comparison between three datasets with 1213, 1738, and 1305 DEGs, revealed a total of 137 common DEGs between GC and normal tissues. B. Network of the top 10 genes, with a higher ranking indicated by a more intense red. C. Genetic mutation analysis of 10 hub genes in GC. D. Expression of THBS2 mRNA in different tumor types including gastric cancer (GC) and normal adjacent tissue, according to TCGA database analysis. E. Relationship between THBS2 and T stage of tumor. F. Expression of THBS2 mRNA in GC according to GEO databases analysis. G, H. Expression of THBS2 mRNA and protein in gastric cancer cell line and GES-1. I. The relative expression level of THBS2 mRNA in 30 pairs of GC and normal adjacent tissues. J, K. THBS2 protein expression and IHC analysis in GC and adjacent normal tissues. L. The prognostic survival of THBS2 was analyzed based on K-M plotter (OS, n=875; FPS, n=640; PPS, n=498). Data represent the mean ± SD. *P < 0.05, **P < 0.01, ***P < 0.001, ns = no significance.

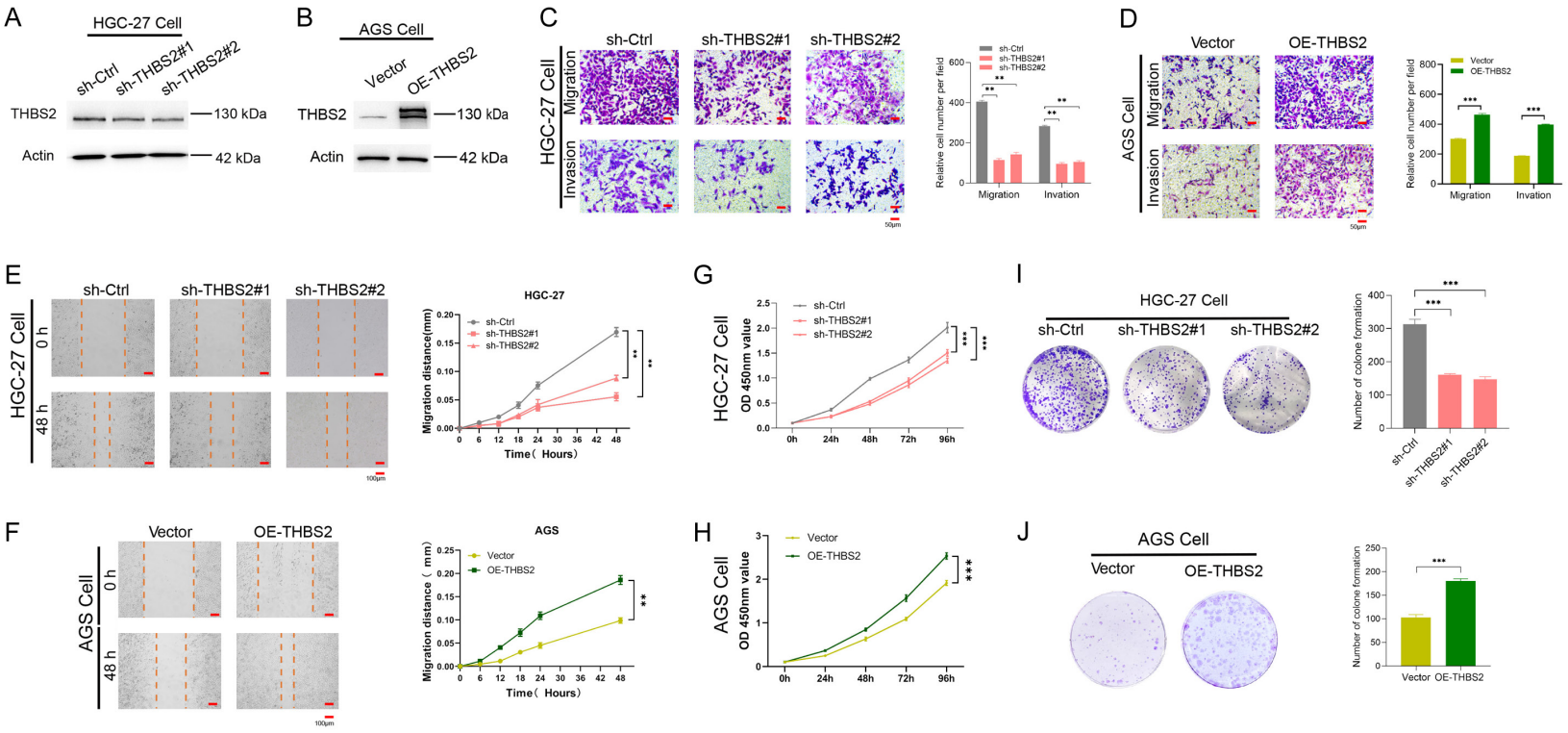
A
HGC-27 Cell
sh-Ctrl
sh-THBS2#1
sh-THBS2#2
THBS2
130 kDa
Actin
42 kDa
B
AGS Cell
Vector
OE-THBS2
THBS2
130 kDa
Actin
42 kDa
C
sh-Ctrl
sh-THBS2#1
sh-THBS2#2
HGC-27 Cell
Migration
Invasion
Relative cell number per field
Migration
Invasion
D
Vector
OE-THBS2
AGS Cell
Migration
Invasion
Relative cell number per field
Migration
Invation
E
sh-Ctrl
sh-THBS2#1
sh-THBS2#2
HGC-27 Cell
0 h
48 h
HGC-27
Migration distance(mm)
Time(Hours)
F
Vector
OE-THBS2
AGS Cell
0 h
48 h
AGS
Migration distance (mm)
Time(Hours)
G
HGC-27 Cell
OD 450nm value
0h
24h
48h
72h
96h
H
AGS Cell
OD 450nm value
Vector
OE-THBS2
I
HGC-27 Cell
sh-Ctrl
sh-THBS2#1
sh-THBS2#2
Number of colone formation
J
AGS Cell
Vector
OE-THBS2
Number of colone formation

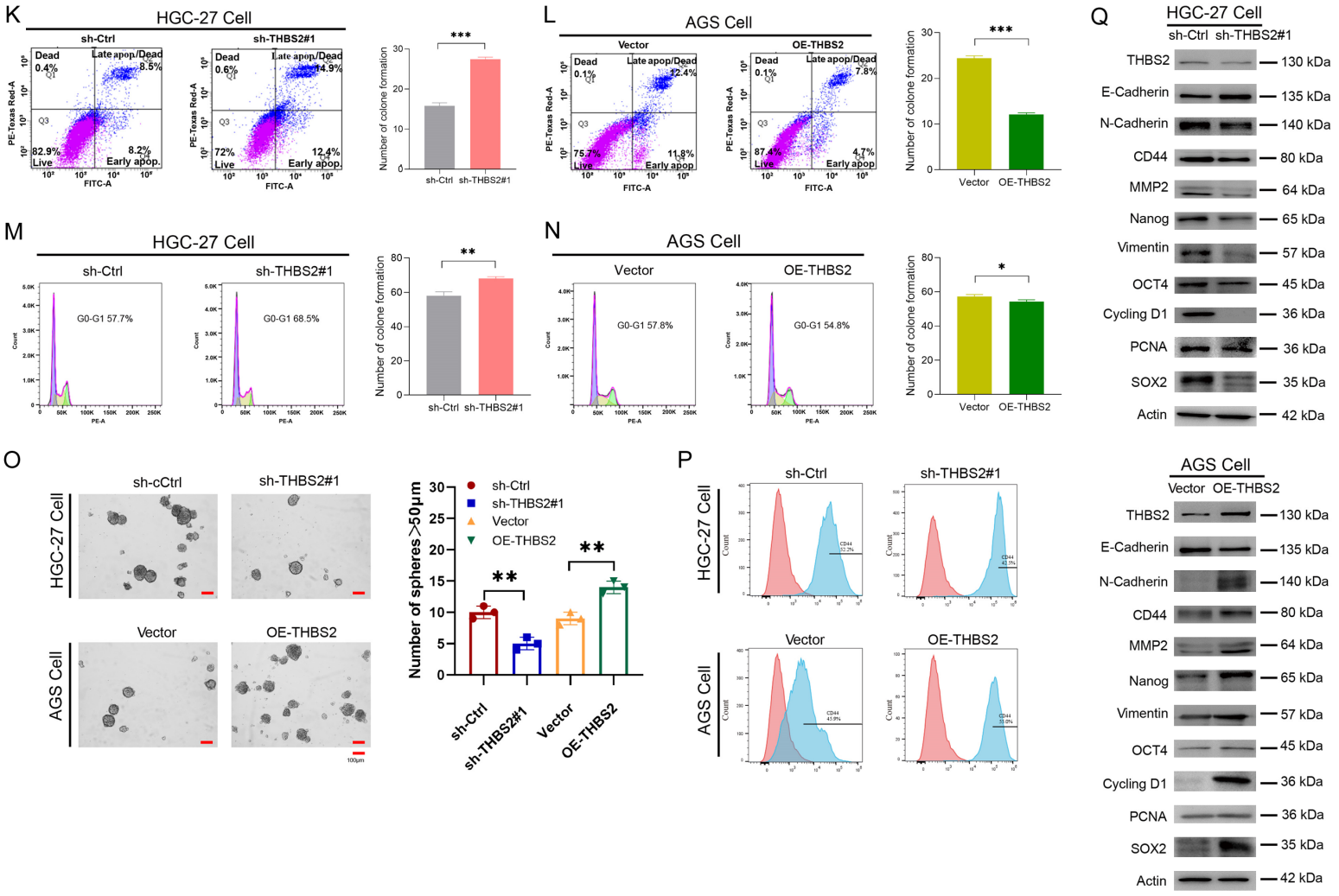

Figure 2. THBS2 regulates the progression and stemness of GC cells in vitro. A, B. WB and qRT-PCR validate the efficiency of constructed THBS2 knockdown and overexpression gastric cancer cell lines. C, D. The migration and invasion ability of sh-THBS2 and OE-THSB2 groups were detected by Transwell assay. E, F. Wound healing assay was used to detect the migration distance of sh-THBS2 and OE-THSB2 groups. G, H. The proliferation ability of sh-THBS2 and OE-THSB2 groups was detected by CCK8 assay. I, J. The proliferative potential of sh-THBS2 and OE-THSB2 groups was verified by colony formation experiment. K, L. Apoptosis assay showed the proportions of apoptotic HGC-27 and AGS cells in sh-THBS2 and OE-THSB2 groups. M, N. The cell cycle of sh-THBS2 and OE-THSB2 groups was detected by flow cytometry. O. The Sphere-forming abilities was detected in HGC-27 and AGS cells after THBS2 intervention. P. The expression of CD44 in HGC-27 and AGS cells after THBS2 intervention was detected by flow cytometry. Q. Expression of proliferation, apoptosis, invasion and EMT-related proteins in HGC-27 and AGS cells after THBS2 intervention. Data represent the mean ± SD. **P < 0.01, ***P < 0.001.

expression impeded the migratory and invasive capacities of HGC-27 cells, whereas enhanced THBS2 expression augmented these properties (**Figure 2C**, **2D**). Wound healing assays (**Figure 2E**, **2F**) further confirmed the effect of THBS2 on the regulating nondirected cellular migration in both HGC-27 and AGS cells. The results of CCK8 and colony formation (**Figure 2G-J**) highlighted the effect of THBS2 on the proliferative capacity of HGC-27 cells. Next, we utilized flow cytometry to assess the apoptosis rate of GC cells. THBS2 knockdown increased apoptosis in HGC-27 cells, while its overexpression decreased apoptosis in AGS cells (**Figure 2K**, **2L**). Additionally, cell cycle analysis demonstrated that THBS2 knockdown reduced proliferation and colony formation, and increased the proportion of GC cells in G0-G1 phase in HGC-27 cells. Conversely, overexpression of THBS2 enhanced AGS cell proliferation ability and colony formation rate, while reducing the G0-G1 phase population (**Figure 2M**, **2N**).

To investigate the impact of THBS2 on the stemness properties of GC cells, we cultured cells in ultra-low attachment six-well plates to induce tumorsphere formation, a key feature of cancer stem cells. Alterations in THBS2 expression markedly affected tumorsphere formation (**Figure 2O**) and CD44 expression, as measured by flow cytometry (**Figure 2P**). Further investigations focused on the influence of THBS2 in proliferation, invasion, EMT, and proteins associated with stemness in both HGC-27 and AGS cell lines following infection with either THBS2 knockdown or overexpression. The findings suggested that THBS2 supported GC tumorigenesis, invasion, EMT process, and stem cell-like properties of GC cells (**Figure 2Q**).

Additional correlation analysis between mRNA levels of various EMT markers and THBS2 expression in GC patients from TCGA confirmed these findings (Supplementary Figure 2A-G). Collectively, our results suggest that THBS2 plays a significant role in promoting the development and maintenance of gastric cancer, particularly influencing its progression and stem-like properties.

MiR-29b-3p directly targeted the 3'-UTR of THBS2 mRNA and downregulated THBS2 in GC

To identify potential miRNAs targeting THBS2 in GC, we employed several bioinformatics tools including TargetScan, miRDB, miRWALK, and Starbase. Through the intersection of prediction results, we identified four candidate miRNAs (miR-519d-3p, miR-29b-3p, miR-107, and miR-103a-3p) (**Figure 3A**). These miRNAs were synthesized as mimics and transfected into various GC cell lines (HGC-27, BGC-803, AGS and MKN-28). Quantitative RT-PCR (qRT-PCR) measured THBS2 mRNA levels post-transfection (**Figure 3B**), generating a heatmap to visualize the percentage reduction in THBS2 mRNA expression (**Figure 3C**). Notably, miR-29b-3p mimics resulted in the most significant downregulation of THBS2 across all tested GC cell lines, corroborated by WB analysis showing a significant reduction in THBS2 protein expression (**Figure 3D**).

Further analysis in the TCGA database highlighted significantly lower relative expression levels of miR-29b-3p in GC compared to normal gastric tissues, particularly in stomach adenocarcinoma (STAD) (**Figure 3E**, **3F**). The expression of miR-29b-3p was quantified in GC cell lines and 30 pairs of GC and normal tissues using qRT-PCR (**Figure 3G**, **3H**). Remarkably, both TCGA database and direct tissue analysis indicated a significant negative correlation between miR-29b-3p and THBS2 levels (**Figure 3I**, **3J**). To elucidate the regulatory mechanism, we analyzed THBS2 mRNA in cells transfected with stable miR-29b-3p mimics and inhibitors. Our observations revealed a downregulation of THBS2 expression in AGS cell lines with miR-29b-3p mimic, while HGC-27 cells with miR-29b-3p inhibitor exhibited elevated levels of THBS2 (**Figure 3K**, **3L**), suggesting a potential regulatory relationship between miR-29b-3p and THBS2 in GC. The target Scan and Starbase databases identified the sequence 426-432 within THBS2 mRNA's 3'-UTR as a potential binding site for miR-29b-3p (**Figure 3M**). Therefore, we utilized dual luciferase reporter assay to confirm the direct interaction between miR-29b-3p and THBS2's 3' untranslated region (UTR). Plasmids containing wild-type (WT) and mutant (MUT) versions of the miR-29b-3p binding sites were constructed and then transfected into HEK239T cells along with either miR-NC or miR-29b-3p mimic. Our findings demonstrated a significant reduction in WT THBS2 luciferase activity, while MUT remained unchanged, indicating specific binding of miR-29b-3p to the THBS2 3'UTR (**Figure 3N**).

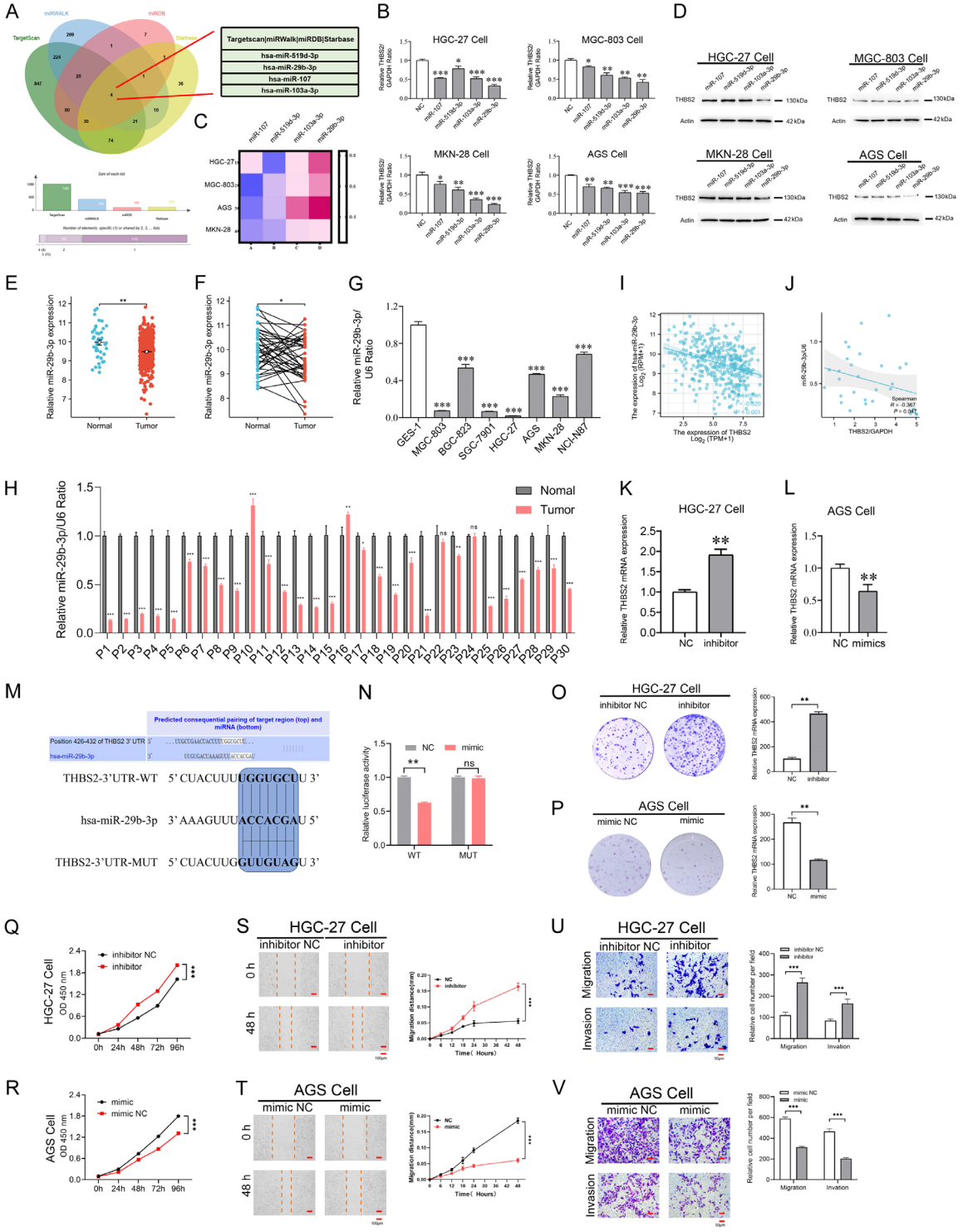

Figure 3. MiR-29b-3p directly targeted the 3'-UTR of THBS2 mRNA and down-regulated THBS2 in GC. A. Bioinformatics predicts THBS2-targeting miRNAs. B. THBS2 mRNA expression of 4 candidate miRNAs transfected into gastric cancer cells. C. The heatmap was drawn to exhibit the decrease extent of THBS2 mRNA. D. The protein expression of THBS2 GC cells after transfection with different kinds of miRNA mimics. E, F. Relative expression of miR-29b-3p in GC and normal tissues in TCGA. G. Expression of THBS2 protein after miR-29b-3p transfected into GC cell lines and GES-1. H. The relative expression level of miR-29b-3p in 30 pairs of GC and normal adjacent tissues. I, J. Correlation between miR-29b-3p andTHBS2 mRNA expression in GC tissues in TCGA and 30 pairs clinic tissues. K, L. The mRNA Expression of THBS2 in HGC-27 and AGS after transfection with miR-29b-3p inhibitor and mimics.

Data represent the mean ± SD. **P < 0.01. M. The potential miR-29b-3p binding sites in 3'-UTR of THBS2 mRNA predicted by TargetScan and the sequences of the WT-THBS2 and MUT-THBS2 3'-UTR reporter plasmids. N. Dual luciferase reporter assay validated of miR-29b-3p targeting THBS2. O, P. Colony formation experiment for AGS and HGC-27 cells with miR-29b-3p mimic or inhibitor. Q, R. CCK8 assay for AGS and HGC-27 cells with miR-29b-3p mimic or inhibitor. S, T. Wound healing assay for AGS and HGC-27 cells with miR-29b-3p mimic or inhibitor. U, V. Transwell assay for AGS and HGC-27 cells with miR-29b-3p mimic or inhibitor. Data represent the mean ± SD. *P < 0.05, **P < 0.01, ***P < 0.001.

To explore the regulatory role of miR-29b-3p in GC cell proliferation and metastasis through THBS2, we conducted functional experiments on GC cells. Specifically, we transfected miR-29b-3p inhibitor and mimic into HGC-27 and AGS cells, respectively. Our findings demonstrated that miR-29b-3p downregulation increased cellular proliferation, as indicated by cell growth assays and colony formation experiments (**Figure 3O**, **3Q**). Conversely, overexpressing miR-29b-3p suppressed GC cell proliferation, as evidenced by CCK8 assay and colony formation assays (**Figure 3P**, **3R**). Moreover, wound healing assay and transwell assay revealed that miR-29b-3p mimic inhibited invasion and migration abilities of GC cells, while miR-29b-3p inhibitor enhanced these capabilities in GC cells (**Figure 3S-V**).

THBS2 reversed miR-29b-3p-mediated inhibition of GC

To further confirm the regulatory relationship between THBS2 and miR-29b-3p, we designed a series of rescue experiments. The results of the WB experiment showed that treatment with a miR-29b-3p inhibitor led to THBS2 expression upregulation, while THBS2 knockdown reversed this phenotype in HGC-27 cells (**Figure 4A**). Moreover, by comparing different treatment groups, we found that THBS2 overexpression can partially reverse the downregulation of THBS2 protein levels caused by miR-29b-3p mimic in AGS cells (**Figure 4B**). Further functional assays including colony formation, wound healing, transwell, and CCK8 assays corroborated that the suppression of THBS2 effectively reversed the tumor-promoting effects initiated by miR-29b-inhibitor (**Figure 4C**, **4E**, **4G**, **4I**).

Then, we introduced a plasmid overexpressing THBS2 and a control vector into AGS cells along with the miR-29b-3p mimic, showing that upregulating THBS2 expression partially counteracted the tumor inhibitory effect induced by miR-29b-3p, as observed by AGS cell proliferation, invasion, and migration assays (**Figure 4D**, **4F**, **4H**, **4J**). These results suggests that miR-29b-3p plays a regulatory role in the functional effects of THBS2 in GC.

THBS2 affects the progression and stemness of GC through Notch signaling pathway

Further exploration of the GSEA dataset underscored a potential role of THBS2 in promoting GC development through the Notch signaling pathway (**Figure 5A**). Notably, Notch3 was found to have the strongest correlation with THBS2, exhibiting a correlation coefficient of 0.622 (P < 0.001) (**Figure 5B**). Furthermore, correlations within Notch signaling pathway markers were extensively investigated using the TCGA database (Supplementary Figure 2H-L). Previous investigations have established a clear association between the Notch signaling pathway and tumor progression as well as the acquisition of cancer stem cell traits [11]. Notch3, notably upregulated in GC, is strongly associated with a poor prognosis [12]. Therefore, we explored whether THBS influences GC progression through the Notch signaling pathway. Initially, WB was employed to assess the expression of key proteins in Notch signaling pathway in GC cells with either knockdown or overexpression of THBS2, respectively. The results revealed that THBS2 knockdown in HGC-27 GC cells reduced the expression of Notch3, NICD, NEY1 and HES1 proteins. Conversely, AGS cells overexpressing THBS2 exhibited increased expression of these proteins (**Figure 5C**).

To verify the importance of notch pathway in the cancer-promoting effect of THBS2, we used Notch pathway inhibitor DAPT, a γ-secretase inhibitor (GSI), which has been shown to effectively curb the oncogenic potential of the Notch signaling [13, 14]. Treatment of THBS2-overexpressing AGS cells with DAPT resulted in inhibition of sphere formation ability induced by THBS2 overexpression (**Figure 5D**). Furthermore, both proliferation and migration abilities were significantly suppressed (Supplementary

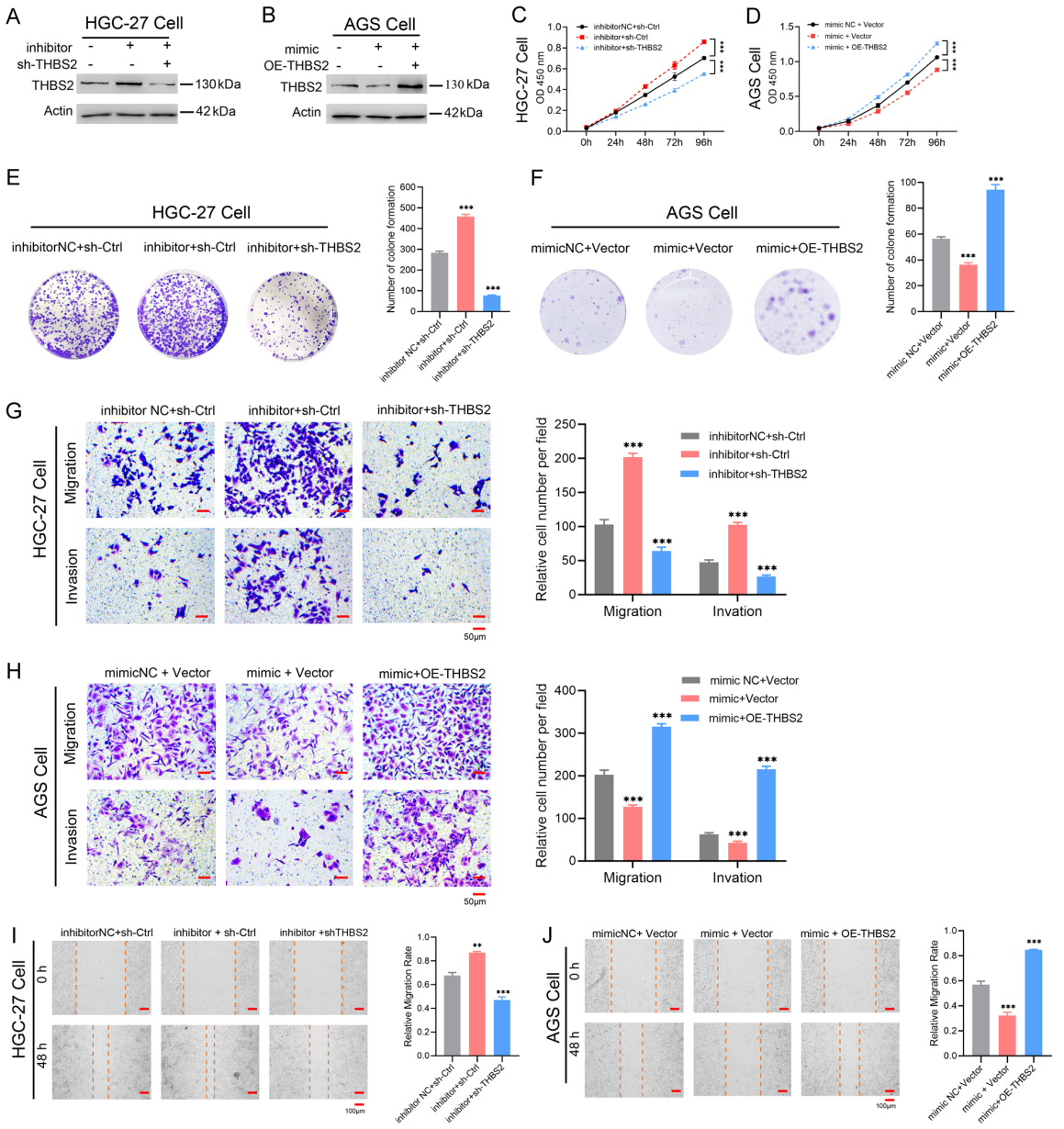

Figure 4. THBS2 reversed Mir-29b-3p-mediated inhibition of GC. A, B. The protein expression of THBS2 in HGC-27 and AGS that co-transfected miR-29b-3p mimic or inhibitor and THBS2 knockdown or overexpression plasmid. C, D. The proliferation of HGC-27 and AGS cells that co-transfected miR-29b-3p mimic or inhibitor and THBS2 knockdown or overexpression plasmid was determined by CCK-8 assay. E, F. The proliferation of HGC-27 and AGS cells that co-transfected miR-29b-3p mimic or inhibitor and THBS2 knockdown or overexpression plasmid was determined by colony formation experiment. G, H. The migration and invasion ability of HGC-27 and AGS cells that co-transfected miR-29b-3p mimic or inhibitor and THBS2 knockdown or overexpression plasmid was determined by transwell assay. I, J. The migration distance of HGC-27 and AGS cells that co-transfected miR-29b-3p mimic or inhibitor and THBS2 knockdown or overexpression plasmid was determined by wound healing assay. Data represent the mean ± SD. **P < 0.01, ***P < 0.001.

Figure 3A, 3C). Subsequent protein expression analysis revealed an increase in THBS2 levels in both the OE-THBS2 and OE-THBS2 + DAPT groups, suggesting that while DAPT does not affect THBS2 expression, it significantly reduces the protein levels of Notch3, Hey1, and HES1. These findings indicate that inhibition of Notch signaling by DAPT can attenuate the impact of THBS2 on invasion, migration, and stemness properties in GC cells (**Figure 5F**).

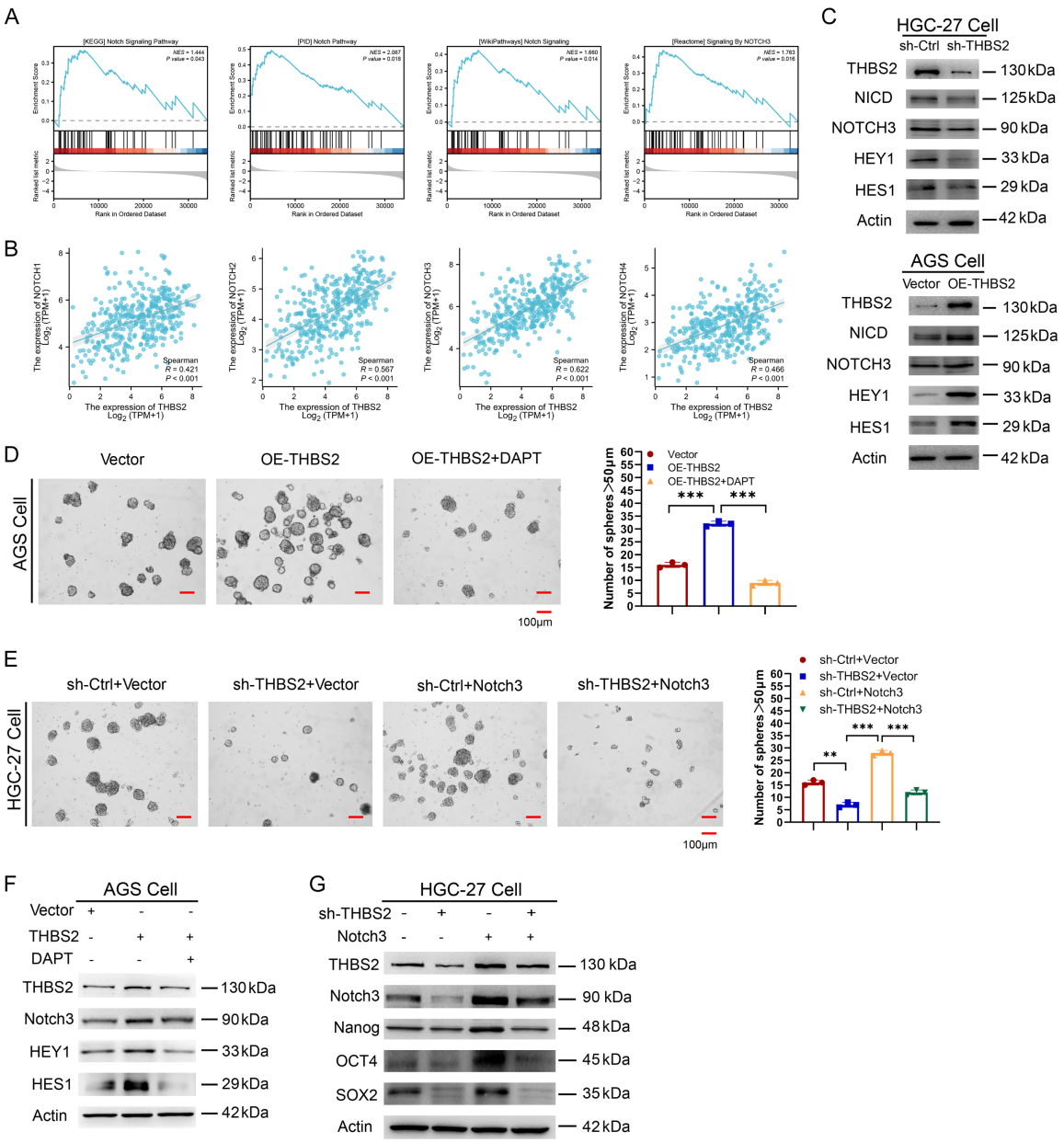

Figure 5. THBS2 affects the progression and stemness of GC through Notch signaling pathway. A. GSEA showed the relationship between the expression of THBS2 and Notch signaling pathway. B. Correlations among THBS2 and Notch1, Notch2, Notch3, and Notch4 analyzed on the basis of TCGA database. C. The protein level of Notch3, Notch target genes or EMT markers (such as NICD, Hey1, Hes1, E-cadherin, N-cadherin, and Vimentin) was assessed in sh-THBS2 and OE-THBS2 groups vs. control by Western Blotting. D. The Sphere-forming abilities was detected in Vector, THBS2 or THBS2 + DAPT groups. Data represent the mean ± SD. ***P < 0.001. E. The Sphere-forming abilities was detected in knockdown THBS2 HGC-27 cells with or without overexpressing Notch3. Data represent the mean ± SD. **P < 0.01. F. The expression levels of Notch3, Hey1 and Hes1 proteins in AGS cell with Vector, OE-THBS2 or OE-THBS2 + DAPT groups were detected by WB. G. The Notch3, Nanog, Sox2, and OCT4 protein expression levels in knockdown THBS2 HGC-27 cells with or without overexpressing Notch3 were analyzed by WB.

To further investigate the mechanism by which THBS2 promotes gastric cancer stem cell (GCSC) phenotype through Notch3, we noticed that the inhibitory effects of THBS2 knockdown on gastric cancer was reinstated by Notch3. Our sphere formation assay indicated that the reduction in stem cell characteristics induced by THBS2 knockdown could be partially

restored through the ectopic expression of Notch3 (**Figure 5E**). Consistent outcomes were observed concerning proliferative and migratory abilities (Supplementary Figure 3B, 3D). WB experiments showed that the reductions in Nanog, OCT4, and SOX2 - proteins specific to stem cells - in GCSCs due to decreased THBS2 expression could be partly reversed upon activation of Notch3 signaling (**Figure 5G**). Collectively, these findings strongly substantiate the role of Notch3 as a crucial downstream regulatory regulator essential for maintaining cancer stem cell-like characteristics driven by THBS2 in GC cells.

Down-regulation of THBS2 inhibits GC tumorigenesis in vivo

To confirm whether THBS2 expression could inhibit the tumorigenesis of GC cells in vivo, we implanted HGC-27 cells infected with a specific shRNA targeting THBS2 or a mock shRNA control into male BALB/c nude mice. Tumor volume was measured every two days starting from 7 days post-injection. At the end of the third week, all mice were sacrificed to evaluate the primary tumors. The results revealed that both tumor weight and size were significantly reduced in the sh-THBS2 group compared to the sh-Ctrl group (**Figure 6A-C**). Additionally, we established an in vivo cancer cell liver metastasis model by injecting GC cells into the spleen. After six weeks, the treatment with sh-THBS2 resulted in a notable decrease in both the volume and number of liver metastatic sites compared to the control group (**Figure 6D**). H&E staining of the livers from the sh-THBS2 group also exhibited smaller tumor metastases compared to the control group (**Figure 6E**). qRT-PCR experiments demonstrated that sh-THBS2 group displayed reduced the expression of Notch3, N-Cadherin, and Vimentin mRNA level, while E-Cadherin protein levels increased (**Figure 6F**). The same conclusion was reached through WB for proteins detection (**Figure 6G**). Building upon these results, we posit that the downregulation of THBS2 can impede the Notch signaling pathway and impede EMT progression in gastric cancer in vivo.

In summary, our findings suggest that, mediated by miR-29b-3p, THBS2 promotes gastric cancer progression and stemness by Notch signaling pathway (**Figure 6H**).

Discussion

Several studies have shown that the THBS family significantly influences the progression of various cancers [6, 15, 16]. Liu revealing the involvement of THBS2 in promoting lung cancer proliferation and migration [10], while knockdown of THBS2 expression reduces cell mobility in lung cancer models. Kim et al. discovered that THBS2 improved the ability of CA19-9 to distinguish PDAC from pancreatitis [17], where the combined detection of THBS2 and CA19-9 reached a specificity of 98% and a sensitivity of 87%. Our study observed a notable upregulation of THBS2 expression in GC tissue samples through qRT-PCR and WB detection, affirming its potential as a potential biomarker and therapeutic target. The correlation between elevated THBS2 expression and poor patient outcomes, underscores its significance as an oncogene across various tumors. Additionally, our findings reveal that targeting THBS2 may effectively impede GC cell migration, invasion, and stem cell-like characteristics, validating its potential as a therapeutic target for GC treatment.

MicroRNAs (miRNAs) are small, single-stranded RNAs (18-22 nt) that naturally occur in vertebrates and function as regulators of cellular protein expression, influencing tissue development, differentiation, cell growth, and apoptosis in both non-cancerous and cancerous cells [18-21]. Our research confirms a direct interaction between THBS2 and miR-29b-3p. Contrary to expectations, while the expression of THBS2 was elevated, miR-29b-3p was downregulated in samples from GC patients. Previous research has highlighted the crucial role of miR-29b-3p in suppressing tumors such as acute myeloid leukemia, colon cancer, and myeloma [21-23]. Pan et al. demonstrated that high levels of miR-29b-3p were associated with improved prognosis for lung adenocarcinoma and invasive breast cancer patients [24], noting that reduced miR-29b-3p enhanced cancer cell invasion and migration and influenced cancer stem cells (CSCs) traits. However, there is limited information regarding the specific function of miR-29b-3p in GC. Our investigation revealed that miR-29b-3p is underexpressed in GC and acts to inhibit tumor progression. Rescue experiments further demonstrated that THBS2 is crucially regulated by miR-29b-3p expression in gastric

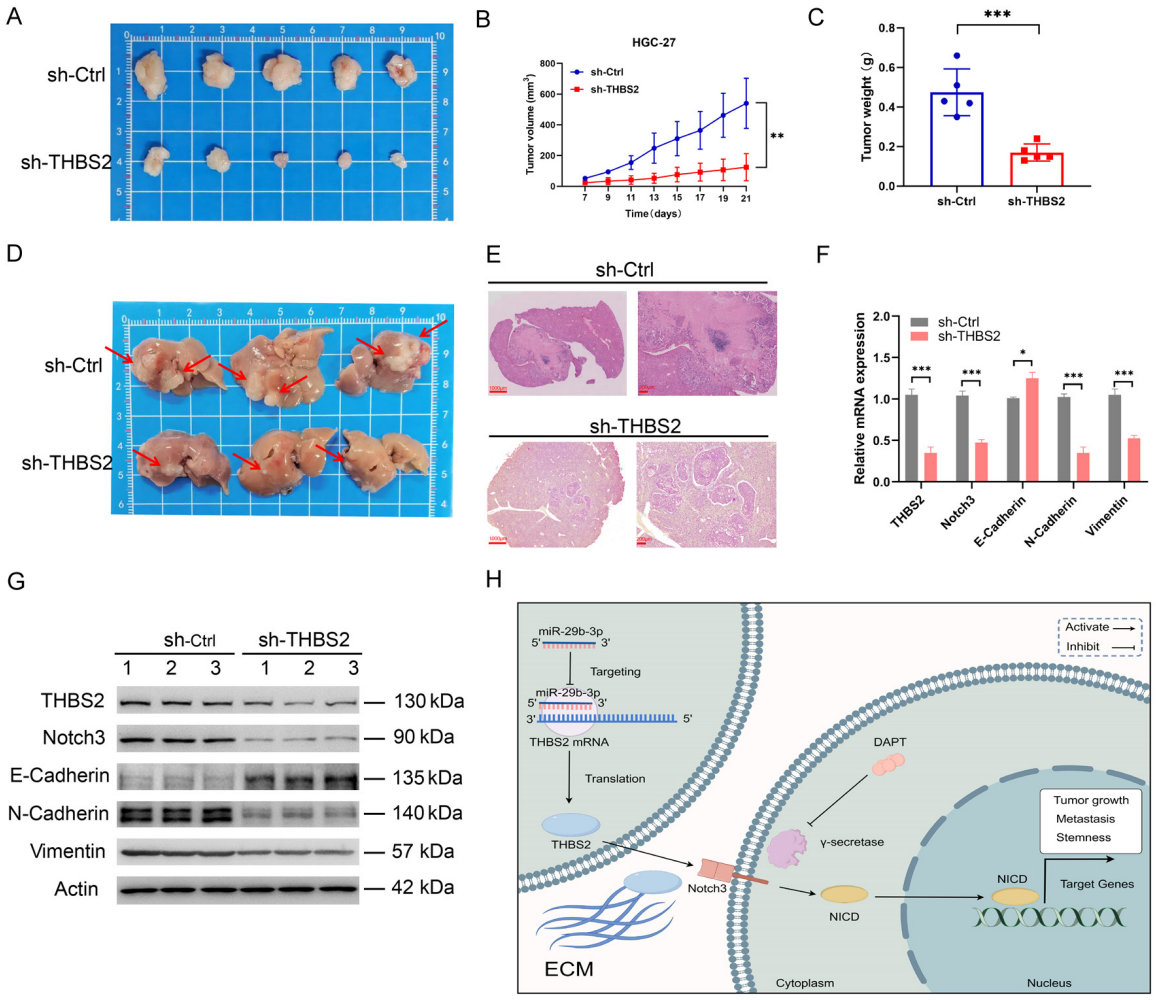

Figure 6. Down-regulation of THBS2 inhibits GC tumorigenesis in vivo. A. Images of tumors from nude mice in the sh-Ctrl and sh-THBS2 groups. B, C. Tumor weights and volumes in the two groups. Data represent the mean ± SD. **P < 0.01, ***P < 0.001. D. Images of liver metastatic tumors after injection of HGC-27 cells (sh-Ctrl and sh-THBS2 groups) into the spleen. E. H&E staining about liver metastasis of spleen injected mice, 2× and 20×. F. The mRNA level of THBS2, EMT markers and Notch3 in established xenograft model assessed by qRT-PCR. Data represent the mean ± SD. *P < 0.05, **P < 0.01, ***P < 0.001. G. The protein level of THBS2, EMT markers and Notch3 in established xenograft model assessed by WB. H. Overall schematic presentation of miR-29b-3p/THBS2/NOTCH3 cascade in gastric carcinogenesis.

cancer, underlining the significant role of miR-29b-3p as a regulator of THBS2 in GC.

GC stem cells (GCSC) are capable of producing daughter tumor cells with robust proliferation ability and heterogeneity through asymmetric division, while the stem cells themselves remain an immature or undifferentiated state, essential for maintaining their self-renewal ability [25, 26]. GCSC is also closely related to the phenomenon of EMT. GCSCs with multidirectional differentiation potential can evolve into tumor cells exhibiting mesenchymal characteristics, thus laying the groundwork for tumor metastasis [27]. Therefore, GCSCs are not only the origin of tumorigenesis, but also play an important role in tumor metastasis, recurrence and chemotherapy resistance. Given the potential correlation between THBS2 and GCSCs, we explored the effects of THBS2 on cancer stem cell-like characteristics. As anticipated, our findings revealed that THBS2 depletion reduced cancer stem cell-like traits, evidenced by decreased spheroid formation assays and lower expression of CSC markers. Conversely, overexpression of THBS2 sustained these cancer stem cell-like features. Moreover, in addition to its role in tumor cell invasion and metas-

tasis, EMT is closely linked to the manifestation of cancer stem cell-like phenotypes. Increasing evidence supports the crucial involvement of EMT in enriching cells with CSC properties [28-30]. Overall, our study highlights the participation of THBS2 in maintaining cancer stem cell-like properties.

Several studies have confirmed the oncogenic and growth-promoting effects associated with Notch signaling, which is implicated in driving various cancers, including colorectal cancer [31], breast cancer [32], and pancreatic cancer [33]. Additionally, the involvement of the Notch signaling pathway in GCSC progression is well-documented [34-38]. Our findings, derived from sphere formation assay, WB, and flow cytometry, confirmed a reduction in the expression of Notch pathway components such as Notch3 and Hey1 sh-THBS2 cells. Previous studies have highlighted the crucial role of Nocth3, Hey1, and HES1 in GC progression [12, 39-41]. Furthermore, recent studies have demonstrated the pivotal function of Notch signaling in activating EMT and promoting GC progression by modulating pathways and transcription factors involved in crosstalk with stem cell characteristics [42]. Our experiments validated the hypothesis that varying expression levels of THBS2 correlate with differential expression of Notch components and EMT markers associated with stem cell properties. Thus, Notch signaling inactivation by a γ-secretase inhibitor such as DAPT [43] may mitigate the CSCS characteristics of THBS2 overexpressing GC. Further experiments confirmed that Notch3 overexpression partially reversed the effect of THBS2 knockdown on stemness markers. However, this aspect of our study is limited and suggests areas for deeper investigation. Additional molecular biology experiments are required to elucidate the underlying mechanisms, such as interactions that activate Notch and EMT signaling pathways in response to THBS2 upregulation.

Furthermore, there is a notable scarcity of research exploring the correlation between THBS2 and GC progression, particularly its association with the Notch pathway. This gap in the literature has also constrained our understanding of the molecular dynamics involved. Some studies have found that THBS2 can amplify the effects of Notch3 pathway activation, which is consistent with our own findings [44]. Consequently, our results may provide a foundational basis for further investigating into both upstream and downstream mechanisms associated with increased THBS2 expression in driving GC progression. The exact relationship between THBS2 and Notch3 remains uncertain - it could be downstream of Notch3 induction or potentially act as an upstream regulator. In summary, our findings robustly suggest that THBS2 contributes to maintaining cancer stem cell-like traits in GC via the Notch pathway.

The present study still encountered several limitations. It primarily relies on in vitro and animal model analyses, necessitating further clinical validation. Moreover, the limited existing research on THBS2 and its interactions with signaling pathways restrict a comprehensive exploration of the molecular mechanisms. Thus, our findings lay the groundwork for future studies aimed to elucidating downstream mechanisms responsible for THBS2 expression upregulation and its role in advancing gastric cancer.

Conclusion

In conclusion, our research reveals that THBS2 promotes the progression and stemness of GC by activating the Notch signaling pathway, a process potentially inhibited by miR-29-3p. These findings highlight the therapeutic potential of targeting the miR-29b-3p/THBS2/Notch axis as a promising strategy for GC treatment.

Acknowledgements

This study was supported by the Youth Independent Innovation Science Fund Project of Chinese PLA General Hospital (22QNCZ014).

Disclosure of conflict of interest

None.

Address correspondence to: Lin Chen and Hongqing Xi, Department of General Surgery, The First Medical Center of Chinese PLA General Hospital, No. 28 Fuxing Road, Beijing 100853, China. E-mail: chenlinbj@sina.com (LC); xihongqing@126.com (HQX)

References

[1] Sung H, Ferlay J, Siegel RL, Laversanne M, Soerjomataram I, Jemal A and Bray F. Global cancer statistics 2020: GLOBOCAN estimates of

incidence and mortality worldwide for 36 cancers in 185 countries. CA Cancer J Clin 2021; 71: 209-249.
[2] Thrift AP, Wenker TN and El-Serag HB. Global burden of gastric cancer: epidemiological trends, risk factors, screening and prevention. Nat Rev Clin Oncol 2023; 20: 338-349.
[3] Wong MCS, Huang J, Chan PSF, Choi P, Lao XQ, Chan SM, Teoh A and Liang P. Global incidence and mortality of gastric cancer, 1980-2018. JAMA Netw Open 2021; 4: e2118457.
[4] Baenziger NL, Brodie GN and Majerus PW. A thrombin-sensitive protein of human platelet membranes. Proc Natl Acad Sci U S A 1971; 68: 240-243.
[5] Adams JC and Lawler J. The thrombospondins. Cold Spring Harb Perspect Biol 2011; 3: a009712.
[6] Petrik J, Lauks S, Garlisi B and Lawler J. Thrombospondins in the tumor microenvironment. Semin Cell Dev Biol 2024; 155: 3-11.
[7] Liao X, Wang W, Yu B and Tan S. Thrombospondin-2 acts as a bridge between tumor extracellular matrix and immune infiltration in pancreatic and stomach adenocarcinomas: an integrative pan-cancer analysis. Cancer Cell Int 2022; 22: 213.
[8] Chen PC, Tang CH, Lin LW, Tsai CH, Chu CY, Lin TH and Huang YL. Thrombospondin-2 promotes prostate cancer bone metastasis by the up-regulation of matrix metalloproteinase-2 through down-regulating miR-376c expression. J Hematol Oncol 2017; 10: 33.
[9] He Z, Lin J, Chen C, Chen Y, Yang S, Cai X, He Y and Liu S. Identification of BGN and THBS2 as metastasis-specific biomarkers and poor survival key regulators in human colon cancer by integrated analysis. Clin Transl Med 2022; 12: e973.
[10] Liu JF, Lee CW, Tsai MH, Tang CH, Chen PC, Lin LW, Lin CY, Lu CH, Lin YF, Yang SH and Chao CC. Thrombospondin 2 promotes tumor metastasis by inducing matrix metalloproteinase-13 production in lung cancer cells. Biochem Pharmacol 2018; 155: 537-546.
[11] Pannuti A, Foreman K, Rizzo P, Osipo C, Golde T, Osborne B and Miele L. Targeting Notch to target cancer stem cells. Clin Cancer Res 2010; 16: 3141-3152.
[12] Kang W, Zhang J, Huang T, Zhou Y, Wong CC, Chan RCK, Dong Y, Wu F, Zhang B, Wu WKK, Chan MWY, Cheng ASL, Yu J, Wong N, Lo KW and To KF. NOTCH3, a crucial target of miR-491-5p/miR-875-5p, promotes gastric carcinogenesis by upregulating PHLDB2 expression and activating Akt pathway. Oncogene 2021; 40: 1578-1594.
[13] Zhou J, Jain S, Azad AK, Xu X, Yu HC, Xu Z, Godbout R and Fu Y. Notch and TGFβ form a positive regulatory loop and regulate EMT in epithelial ovarian cancer cells. Cell Signal 2016; 28: 838-849.
[14] Huang T, Zhou Y, Cheng AS, Yu J, To KF and Kang W. NOTCH receptors in gastric and other gastrointestinal cancers: oncogenes or tumor suppressors? Mol Cancer 2016; 15: 80.
[15] Kazerounian S, Yee KO and Lawler J. Thrombospondins in cancer. Cell Mol Life Sci 2008; 65: 700-712.
[16] Huang J, Wang C, Hou Y, Tian Y, Li Y, Zhang H, Zhang L and Li W. Molecular mechanisms of thrombospondin-2 modulates tumor vasculogenic mimicry by PI3K/AKT/mTOR signaling pathway. Biomed Pharmacother 2023; 167: 115455.
[17] Kim J, Bamlet WR, Oberg AL, Chaffee KG, Donahue G, Cao XJ, Chari S, Garcia BA, Petersen GM and Zaret KS. Detection of early pancreatic ductal adenocarcinoma with thrombospondin-2 and CA19-9 blood markers. Sci Transl Med 2017; 9: eaah5583.
[18] Calin GA and Croce CM. MicroRNA signatures in human cancers. Nat Rev Cancer 2006; 6: 857-866.
[19] He L, He X, Lowe SW and Hannon GJ. microRNAs join the p53 network--another piece in the tumour-suppression puzzle. Nat Rev Cancer 2007; 7: 819-822.
[20] Stefani G and Slack FJ. Small non-coding RNAs in animal development. Nat Rev Mol Cell Biol 2008; 9: 219-230.
[21] Konishi H, Sato H, Takahashi K and Fujiya M. Tumor-progressive mechanisms mediating miRNA-protein interaction. Int J Mol Sci 2021; 22: 12303.
[22] Poudyal D, Cui X, Le PM, Hofseth AB, Windust A, Nagarkatti M, Nagarkatti PS, Schetter AJ, Harris CC and Hofseth LJ. A key role of microRNA-29b for the suppression of colon cancer cell migration by American ginseng. PLoS One 2013; 8: e75034.
[23] Rossi M, Pitari MR, Amodio N, Di Martino MT, Conforti F, Leone E, Botta C, Paolino FM, Del Giudice T, Iuliano E, Caraglia M, Ferrarini M, Giordano A, Tagliaferri P and Tassone P. miR-29b negatively regulates human osteoclastic cell differentiation and function: implications for the treatment of multiple myeloma-related bone disease. J Cell Physiol 2013; 228: 1506-1515.
[24] Tang YJ, Wu W, Chen QQ, Liu SH, Zheng ZY, Cui ZL, Xu JP, Xue Y and Lin DH. miR-29b-3p suppresses the malignant biological behaviors of AML cells via inhibiting NF-κB and JAK/STAT signaling pathways by targeting HuR. BMC Cancer 2022; 22: 909.
[25] Houghton J, Stoicov C, Nomura S, Rogers AB, Carlson J, Li H, Cai X, Fox JG, Goldenring JR and

Wang TC. Gastric cancer originating from bone marrow-derived cells. Science 2004; 306: 1568-1571.

[26] Kasashima H, Yashiro M, Nakamae H, Masuda G, Kinoshita H, Morisaki T, Fukuoka T, Hasegawa T, Sakurai K, Toyokawa T, Kubo N, Tanaka H, Muguruma K, Ohira M, Nakane T, Hino M and Hirakawa K. Bone marrow-derived stromal cells are associated with gastric cancer progression. Br J Cancer 2015; 113: 443-452.

[27] Sato R, Semba T, Saya H and Arima Y. Concise review: stem cells and epithelial-mesenchymal transition in cancer: biological implications and therapeutic targets. Stem Cells 2016; 34: 1997-2007.

[28] Mani SA, Guo W, Liao MJ, Eaton EN, Ayyanan A, Zhou AY, Brooks M, Reinhard F, Zhang CC, Shipitsin M, Campbell LL, Polyak K, Brisken C, Yang J and Weinberg RA. The epithelial-mesenchymal transition generates cells with properties of stem cells. Cell 2008; 133: 704-715.

[29] Thiery JP, Acloque H, Huang RY and Nieto MA. Epithelial-mesenchymal transitions in development and disease. Cell 2009; 139: 871-890.

[30] Battula VL, Evans KW, Hollier BG, Shi Y, Marini FC, Ayyanan A, Wang RY, Brisken C, Guerra R, Andreeff M and Mani SA. Epithelial-mesenchymal transition-derived cells exhibit multilineage differentiation potential similar to mesenchymal stem cells. Stem Cells 2010; 28: 1435-1445.

[31] Jackstadt R, van Hooff SR, Leach JD, Cortes-Lavaud X, Lohuis JO, Ridgway RA, Wouters VM, Roper J, Kendall TJ, Roxburgh CS, Horgan PG, Nixon C, Nourse C, Gunzer M, Clark W, Hedley A, Yilmaz OH, Rashid M, Bailey P, Biankin AV, Campbell AD, Adams DJ, Barry ST, Steele CW, Medema JP and Sansom OJ. Epithelial NOTCH signaling rewires the tumor microenvironment of colorectal cancer to drive poor-prognosis subtypes and metastasis. Cancer Cell 2019; 36: 319-336, e7.

[32] Leontovich AA, Jalalirad M, Salisbury JL, Mills L, Haddox C, Schroeder M, Tuma A, Guicciardi ME, Zammataro L, Gambino MW, Amato A, Di Leonardo A, McCubrey J, Lange CA, Liu M, Haddad T, Goetz M, Boughey J, Sarkaria J, Wang L, Ingle JN, Galanis E and D'Assoro AB. NOTCH3 expression is linked to breast cancer seeding and distant metastasis. Breast Cancer Res 2018; 20: 105.

[33] Avila JL and Kissil JL. Notch signaling in pancreatic cancer: oncogene or tumor suppressor? Trends Mol Med 2013; 19: 320-327.

[34] Fu Y, Li H and Hao X. The self-renewal signaling pathways utilized by gastric cancer stem cells. Tumour Biol 2017; 39: 1010428317697577.

[35] Kim YS, Lee HJ, Park JM, Han YM, Kangwan N, Oh JY, Lee DY and Hahm KB. Targeted molecular ablation of cancer stem cells for curing gastrointestinal cancers. Expert Rev Gastroenterol Hepatol 2017; 11: 1059-1070.

[36] Bekaii-Saab T and El-Rayes B. Identifying and targeting cancer stem cells in the treatment of gastric cancer. Cancer 2017; 123: 1303-1312.

[37] Miao ZF, Xu H, Xu HM, Wang ZN, Zhao TT, Song YX and Xu YY. DLL4 overexpression increases gastric cancer stem/progenitor cell self-renewal ability and correlates with poor clinical outcome via Notch-1 signaling pathway activation. Cancer Med 2017; 6: 245-257.

[38] Papadakos KS, Bartoschek M, Rodriguez C, Gialeli C, Jin SB, Lendahl U, Pietras K and Blom AM. Cartilage oligomeric matrix protein initiates cancer stem cells through activation of Jagged1-Notch3 signaling. Matrix Biol 2019; 81: 107-121.

[39] Kang H, An HJ, Song JY, Kim TH, Heo JH, Ahn DH and Kim G. Notch3 and Jagged2 contribute to gastric cancer development and to glandular differentiation associated with MUC2 and MUC5AC expression. Histopathology 2012; 61: 576-586.

[40] Zheng L, Cao J, Liu L, Xu H, Chen L, Kang L and Gao L. Long noncoding RNA LINC00982 upregulates CTSF expression to inhibit gastric cancer progression via the transcription factor HEY1. Am J Physiol Gastrointest Liver Physiol 2021; 320: G816-G828.

[41] Li L, Li Y, Wang L, Wu Z, Ma H, Shao J, Li D, Yu H, Nian W and Wang D. Inhibition of Hes1 enhances lapatinib sensitivity in gastric cancer sphere-forming cells. Oncol Lett 2017; 14: 3989-3996.

[42] Hibdon ES, Razumilava N, Keeley TM, Wong G, Solanki S, Shah YM and Samuelson LC. Notch and mTOR signaling pathways promote human gastric cancer cell proliferation. Neoplasia 2019; 21: 702-712.

[43] Li LC, Peng Y, Liu YM, Wang LL and Wu XL. Gastric cancer cell growth and epithelialmesenchymal transition are inhibited by γ-secretase inhibitor DAPT. Oncol Lett 2014; 7: 2160-2164.

[44] Meng H, Zhang X, Hankenson KD and Wang MM. Thrombospondin 2 potentiates notch3/jagged1 signaling. J Biol Chem 2009; 284: 7866-7874.

Supplementary Table 1. RT-PCR primers of mRNA and miRNA

Gene	Species	Category	Sequence (5'-3')
THBS2	Human	Sense	CCTACATCTCCAACGCCAACCAG
THBS2	Human	Antisense	CCATCACCGTCCAAGTCCTCCT
has-miR-29b-3p	Human	RT	GTCGTATCCAGTGCAGGGTCCGAGG TATTCGCACTGGATACGACAACACT
has-miR-29b-3p	Human	Sense	CGCGTAGCACCATTTGAAATC
has-miR-29b-3p	Human	Antisense	AGTGCAGGGTCCGAGGTATT
U6	Human	Sense	CGCTTCGGCAGCACATATAC
U6	Human	Antisense	AACGCTTCACGAATTTGCGT
has-miR-519d-3p mimic	Human	Sense	CAAAGUGCCUCCCUUUAGAGUG
has-miR-519d-3p mimic	Human	Antisense	CACUCUAAAGGGAGGCACUUUG
has-miR-29b-3p mimic	Human	Sense	UAGCACCAUUUGAAAUCAGUGUU
has-miR-29b-3p mimic	Human	Antisense	AACACUGAUUUCAAAUGGUGCUA
has-miR-107 mimic	Human	Sense	AGCAGCAUUGUACAGGGCUAUCA
has-miR-107 mimic	Human	Antisense	UGAUAGCCCUGUACAAUGCUGCU
has-miR-103a-3p mimic	Human	Sense	AGCAGCAUUGUACAGGGCUAUGA
has-miR-103a-3p mimic	Human	Antisense	UCAUAGCCCUGUACAAUGCUGCU
has-miR-29b-3p inhibitor	Human	--	AACACUGAUUUCAAAUGGUGCUA
THBS2 sh#1	Human	Sense	CCACGUGUACCUGCAAGAAAUTT
THBS2 sh#1	Human	Antisense	AUUUCUUGCAGGUACACGUGGTT
THBS2 sh#2	Human	Sense	GGACGAUGUCUUCAAUGAATT
THBS2 sh#2	Human	Antisense	UUCAUUGAAGACAUCGUCCTT
Notch3	Human	Sense	CTCTTACTGGTCGTCGTTCT
Notch3	Human	Antisense	TGCCTCATCCTCTTCAGTTG
E-cadherin	Human	Sense	TCCTAATAGCAACCACAGTCACTG
E-cadherin	Human	Antisense	TTTCAGTGTGGTGATTACGACGTTA
N-cadherin	Human	Sense	TGAGGAGTCAATTCCAACCGA
N-cadherin	Human	Antisense	GGCAAGTTGATTGGAGGGATG
Vimentin	Human	Sense	GAGTAACCAAGGAAATTCCCGTAG
Vimentin	Human	Antisense	GGCGGCCAATAGTGTCTTGGTAG

Supplementary Table 2. Details of antibodies used in this study

Company	Catalog number	Antibody	Specificity	WB/IHC dilution
BOSTER	BA3616-2	THBS2	Rabbit	1:1000 (WB)
BOSTER	BA3616-2	THBS2	Rabbit	1:1000 (IHC)
Bioswamp	PAB38363	NOTCH3	Rabbit	1:1000
Bioswamp	PAB44274	NICD	Rabbit	1:500
Bioswamp	PAB32844	HEY1	Rabbit	1:1000
Bioswamp	PAB37469	HES1	Rabbit	1:1000
Bioswamp	PAB33609	Nanog	Rabbit	1:1000
CST	14472	E-Cadherin	Rabbit	1:1000
CST	13116	N-Cadherin	Rabbit	1:1000
CST	5741	Vimentin	Rabbit	1:1000
CST	40994	MMP2	Rabbit	1:1000
CST	3570	CD44	Rabbit	1:1000
CST	2750	OCT4	Rabbit	1:1000
CST	3579	SOX2	Rabbit	1:1000
CST	55506	Cycling D1	Rabbit	1:1000
CST	2586	PCNA	Rabbit	1:1000
ABclonal	AC004	Actin	Mouse	1:10000
ZSGB-BIO	ZB-5301	Secondary antibodies	Rabbit	1:5000
ZSGB-BIO	ZB-5305	Secondary antibodies	Mouse	1:5000
BD	560533	Hu CD44 PE-Cy7 G44-26 PMGst		

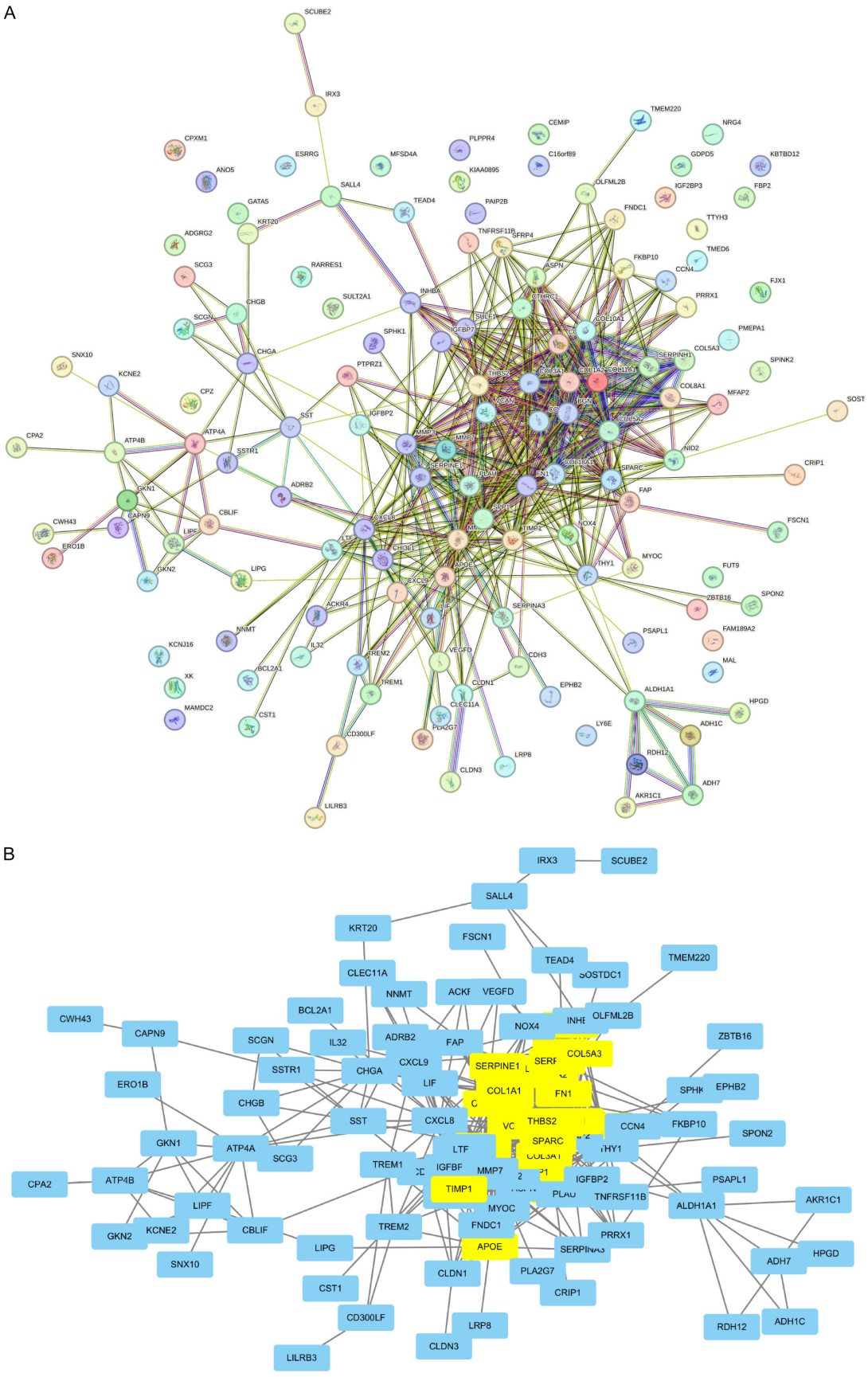
A
SCUBE2
IRX3
CPXM1
ESRRG
MFSD4A
PLPPR4
CEMIP
TMEM220
NRG4
ANO5
KIAA0895
C16orf89
GDPD5
KBTBD12
SALL4
TEAD4
PAIP2B
OLFML2B
IGF2BP3
FBP2
GATA5
KRT20
FNDC1
TTYH3
ADGRG2
TNFRSF11B
SFRP4
TMED6
SCG3
RARRES1
ASPN
FKBP10
CCN4
FJX1
SULT2A1
INHBA
PRRX1
CHGB
SCGN
SPHK1
IGFBP7
PMEPA1
SNX10
CHGA
COL5A3
KCNE2
PTPRZ1
SERPINH1
SPINK2
CPZ
COL8A1
MFAP2
SOST
SST
IGFBP2
CPA2
ATP4B
ATP4A
MMP3
SSTR1
NID2
CRIP1
SERPINE1
SPARC
GKN1
ADRB2
FAP
CWH43
CAPN9
CBLIF
CXCL9
TIMP1
NOX4
FSCN1
LIPF
ERO1B
CHGA
THY1
MYOC
GKN2
LIPG
APOE
FUT9
CXCL8
ZBTB16
SPON2
ACKR4
LIF
SERPINA3
NNMT
PSAPL1
FAM189A2
KCNJ16
IL32
VEGFD
CDH3
MAL
XK
BCL2A1
TREM2
EPHB2
TREM1
CLDN1
ALDH1A1
HPGD
MAMDC2
CLEC11A
ADH1C
CST1
PLA2G7
LY6E
CD300LF
RDH12
LRP8
CLDN3
ADH7
AKR1C1
LILRB3
B
IRX3
SCUBE2
SALL4
KRT20
FSCN1
TEAD4
TMEM220
CLEC11A
SOSTDC1
NNMT
VEGFD
BCL2A1
CWH43
CAPN9
NOX4
OLFML2B
SCGN
IL32
ADRB2
FAP
ZBTB16
SSTR1
CHGA
CXCL9
SERPINE1
COL5A3
ERO1B
LIF
COL1A1
FN1
EPHB2
CHGB
SST
CXCL8
THBS2
CCN4
FKBP10
SPON2
GKN1
ATP4A
SCG3
SPARC
LTF
TREM1
IGFBP2
PSAPL1
CPA2
ATP4B
TIMP1
TNFRSF11B
AKR1C1
LIPF
MYOC
ALDH1A1
GKN2
KCNE2
CBLIF
TREM2
FNDC1
PRRX1
LIPG
APOE
HPGD
SNX10
CLDN1
ADH7
CST1
PLA2G7
CRIP1
CD300LF
LRP8
RDH12
ADH1C
CLDN3
LILRB3

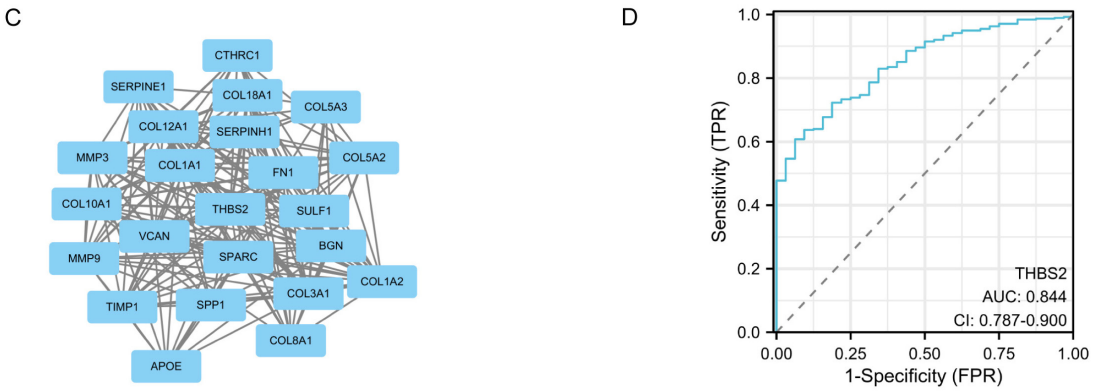

Supplementary Figure 1. A. PPI network was analyzed using the STRING database. B. PPI network was produced using Cytoscope Software. C. Core modules were designed using MCODE application. D. The receiver operator characteristic (ROC) curve analyses of THBS2.

Supplementary Table 3. The relationship between THBS2 and clinicopathological features in GC patients

Characteristics	Low expression of THBS2	High expression of THBS2	*P* value
n	187	188	
Gender, n (%)			0.969
Female	67 (17.9%)	67 (17.9%)	
Male	120 (32%)	121 (32.3%)	
Age, n (%)			0.365
≤ 65	77 (20.8%)	87 (23.5%)	
> 65	107 (28.8%)	100 (27%)	
Race, n (%)			0.013
Asian	42 (13%)	32 (9.9%)	
Black or African American	9 (2.8%)	2 (0.6%)	
White	105 (32.5%)	133 (41.2%)	
Hpylori infection, n (%)			0.440
No	94 (57.7%)	51 (31.3%)	
Yes	10 (6.1%)	8 (4.9%)	
Reflux history, n (%)			0.199
No	97 (45.3%)	78 (36.4%)	
Yes	26 (12.1%)	13 (6.1%)	
Pathologic T stage, n (%)			0.009
T1 & T2	61 (16.6%)	38 (10.4%)	
T3	84 (22.9%)	84 (22.9%)	
T4	40 (10.9%)	60 (16.3%)	
Pathologic N stage, n (%)			0.907
N0	56 (19.8%)	55 (19.4%)	
N1 & N2	88 (31.1%)	84 (29.7%)	
Pathologic M stage, n (%)			0.893
M0	167 (47%)	163 (45.9%)	
M1	13 (3.7%)	12 (3.4%)	
Pathologic stage, n (%)			0.658
Stage I & Stage II	85 (24.1%)	79 (22.4%)	
Stage III & Stage IV	93 (26.4%)	95 (27%)	
Histologic grade, n (%)			0.002
G1 & G2	88 (24%)	59 (16.1%)	
G3	95 (26%)	124 (33.9%)	
Residual tumor, n (%)			0.781
R0	152 (46.2%)	146 (44.4%)	
R1 & R2	15 (4.6%)	16 (4.9%)	

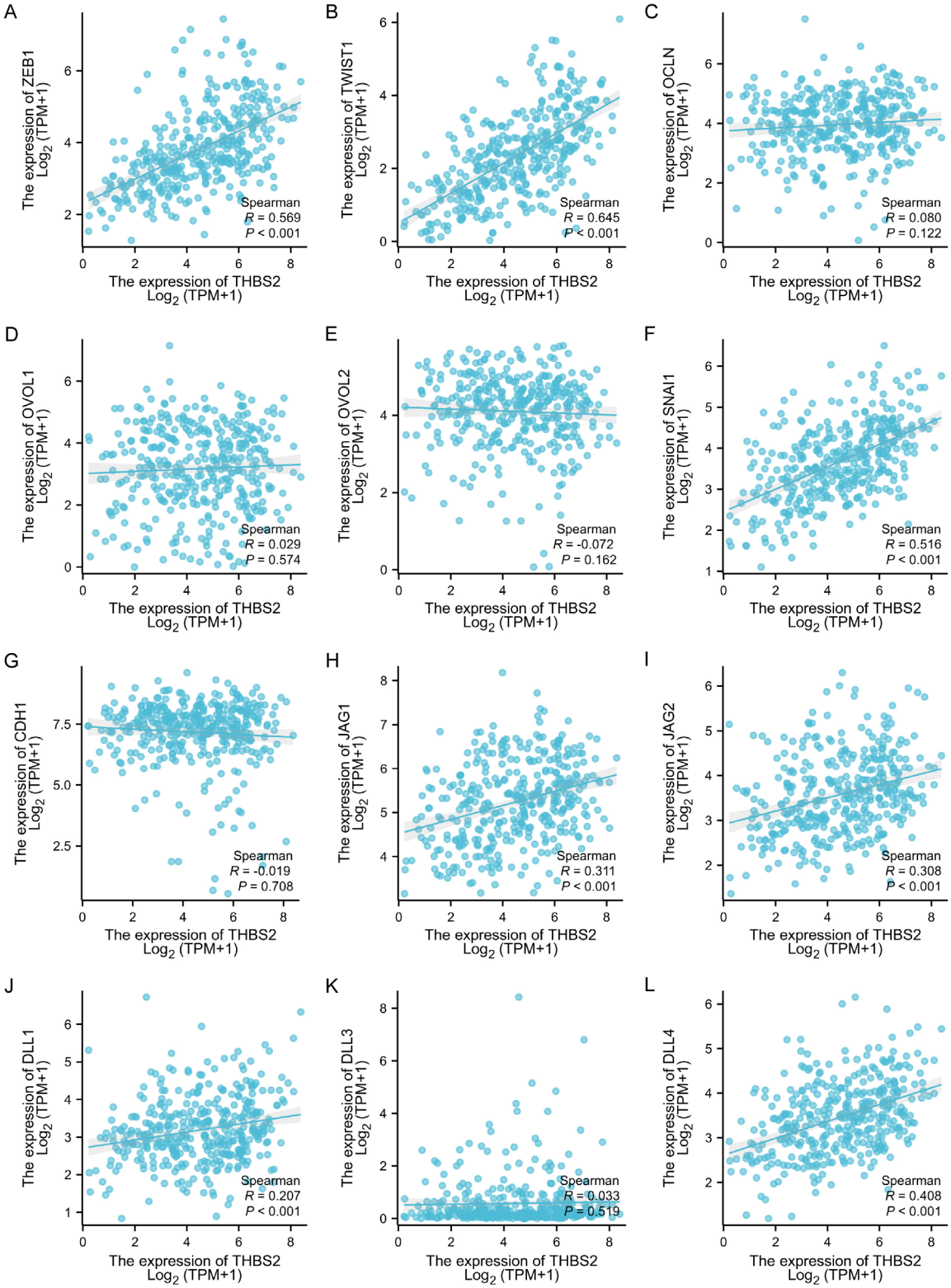

Supplementary Figure 2. A-G. Correlation between THBS2 and various EMT markers. H-L. Correlation between THBS2 and markers in Notch signaling pathway.

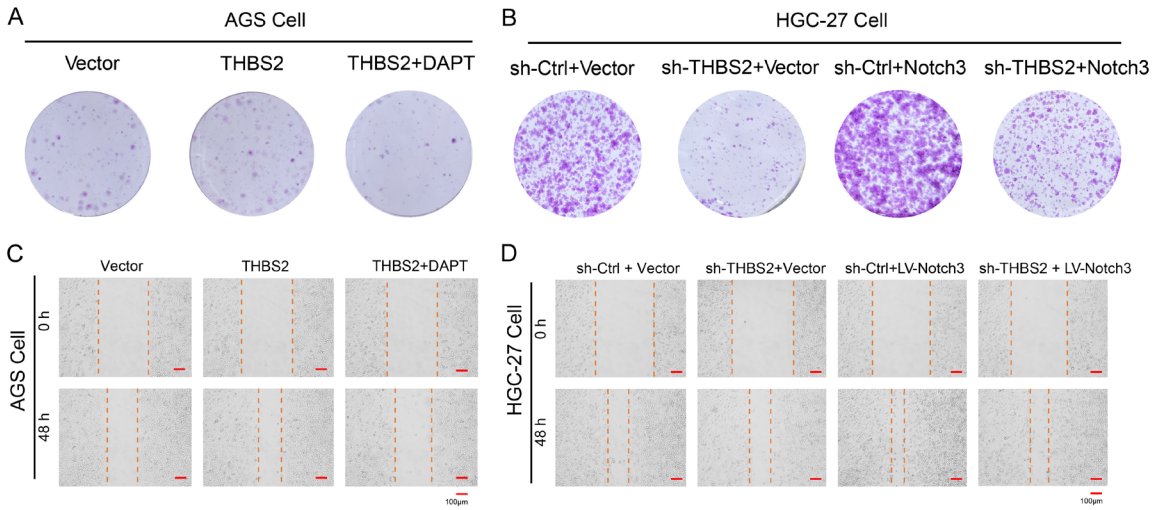

Supplementary Figure 3. A. Colony formation experiment was detected in AGS cell Vector, THBS2 or THBS2 + DAPT groups. B. Colony formation experiment was detected in knockdown THBS2 HGC-27 cells with or without overexpressing Notch3. C. Wound healing assay was detected in AGS cell Vector, OE-THBS2 or OE-THBS2 + DAPT groups. D. Wound healing assay was detected in knockdown THBS2 HGC-27 cells with or without overexpressing Notch3.